

Automatic building information model reconstruction in high-density urban areas: Augmenting multi-source data with architectural knowledge

Ke Chen¹, Weisheng Lu², Fan Xue³, Pingbo Tang⁴, and Ling Hin Li⁵

¹ Post-doctoral Fellow, Department of Real Estate and Construction, Faculty of Architecture, The University of Hong Kong, Hong Kong, leochen@connect.hku.hk;

² Associate Professor, Department of Real Estate and Construction, Faculty of Architecture, The University of Hong Kong, Hong Kong, wilsonlu@hku.hk;

³ Research Assistant Professor, Department of Real Estate and Construction, Faculty of Architecture, The University of Hong Kong, Hong Kong, xuef@hku.hk;

⁴ Assistant Professor, Del E. Webb School of Construction, Arizona State University, USA, tangpingbo@asu.edu;

⁵ Associate Professor, Department of Real Estate and Construction, Faculty of Architecture, The University of Hong Kong, Hong Kong, lhli@hku.hk;

This is the peer-reviewed post-print version of the paper:

Chen, K., Lu, W., Xue, F., Tang, P., & Li, L. H. (2018). Automatic building information model reconstruction in high-density urban areas: Augmenting multi-source data with architectural knowledge. *Automation in Construction*, 93, 22-34.

Doi: [10.1016/j.autcon.2018.05.009](https://doi.org/10.1016/j.autcon.2018.05.009)

The final version of this paper is available at: <https://doi.org/10.1016/j.autcon.2018.05.009>.

The use of this file must follow the [Creative Commons Attribution Non-Commercial No Derivatives License](#), as required by [Elsevier's policy](#).

Abstract: Many studies have been conducted to create building information models (BIMs) or city information models (CIMs) as the digital infrastructure to support various smart city programs. However, automatic generation of such models for high-density (HD) urban areas remains a challenge owing to (a) complex topographic conditions and noisy data irrelevant to the buildings, and (b) exponentially growing computational complexity when the task is reconstructing hundreds of buildings at an urban scale. This paper develops a method — multi-Source rectification of gEometric Primitives (mSTEP) — for automatic reconstruction of BIMs in HD urban areas. By retrieving building base, height, and footprint geodata from topographic maps, level of detail 1 (LoD1) BIMs representing buildings with flat roof configuration were first constructed. Geometric primitives were then detected from LiDAR point clouds and rectified using architectural knowledge about building geometries (e.g. a rooftop object would normally be in parallel with the outer edge of the roof). Finally, the rectified primitives were used to refine the LoD1 BIMs to LoD2, which show detailed geometric features of roofs and rooftop objects. A total of 1,361 buildings located in a four square kilometer area of Hong Kong Island were selected as the subjects for this study. The

evaluation results show that mSTEP is an efficient BIM reconstruction method that can significantly improve the level of automation and decrease the computation time. mSTEP is also well applicable to point clouds of various densities. The research is thus of profound significance; other cities and districts around the world can easily adopt mSTEP to reconstruct their own BIMs/CIMs to support their smart city programs.

Keywords: building information model; city information model; LiDAR point clouds; topographic map; architecture; high-density city

1. Introduction

City reconstruction in 3D digital format emerges popularity in the era of information (Heo *et al.* 2013). A city information model (CIM) contains spatial data and virtual representations of all objects of interest in an urban area. A well-developed CIM can facilitate the work of city planners and urban designers in addressing urban problems such as traffic congestion, accessibility, connectivity, and the potential impact of natural disasters (AECbytes 2016). From a city administrator's perspective, a CIM with rich information can be useful for city governance, while at the individual citizen level, a CIM enables applications such as transportation navigation, emergency response, and many other location-based services. Cities such as New York, London, Berlin, and Adelaide have all created their CIMs to support many of the applications cited above (Over *et al.* 2010; Gröger and Plümer 2012; Sun and Salvaggio 2013).

Buildings are the most important manmade objects in the urban scene (Henricsson and Baltsavias, 1997). Many studies, over the years, have focused on the reconstruction of building information models (BIMs) (*e.g.* Tang *et al.* 2010; Xue *et al.* 2018) which can be stitched together to form a CIM. Another approach is to create CIMs using Geographic Information Systems (GIS) (Li *et al.* 2015) and remote sensing (Haala and Kada 2010; Lillesand *et al.* 2015). In these CIMs, individual buildings could be roughly represented by prisms or “boxes” without precise information on the “as-is” condition. With the advancements of data acquisition and processing technologies, the trend is to reconstruct BIMs that contain detailed geometric features of roofs and rooftop objects (so termed as Level of Detail 2 [LoD2] defined by the Open Geospatial Consortium [OGC] [2012]) to extend CIM applications, *e.g.* green roof development (Choi *et al.* 2017) and energy performance improvement (Yang and Zou 2016).

However, the reconstruction of BIMs, particularly those with greater details, is labor-intensive, time-consuming, and error-prone (Volk *et al.* 2014). The process requires a considerable amount of manual rectifications and computational power, and this becomes extreme burdensome when the task is at the urban scale (Sun and Salvaggio 2013; Li *et al.* 2016; Wu *et al.* 2017).

Researchers have attempted to improve the efficiency of BIM reconstruction by introducing automatic or semi-automatic approaches. Images, 3D laser scanning point clouds, and total station surveying data are commonly used for model reconstruction (*e.g.* Awrangjeb *et al.* 2013; Li *et al.* 2016; Wu *et al.* 2017). Algorithms have been developed to process different types of data and reconstruct BIMs (*e.g.* Heo *et al.* 2013; Xue *et al.* 2018). In addition, with data from multiple sources become affordable, it is now possible to use multi-source data to overcome some of the inherent problems (*e.g.* inaccurate/"noisy" data, incomplete information) associated with single-source data (*e.g.* Habib *et al.* 2010; Cheng *et al.* 2011; Gilani *et al.* 2016). Acknowledging considerable achievements in the field of BIM/CIM reconstruction, BIM/CIM reconstruction in high-density (HD) urban areas remains an open problem (Musialski *et al.* 2013). Firstly, city features such as trees, roads, and terrain introduce a lot of noise that undermines the quality of the measurement data. Secondly, densely-distributed buildings make it difficult to segment data for generating individual BIMs. Lastly, reconstructing thousands of buildings at an urban scale exponentially increases the computational complexity, bringing many difficulties for methods which rely on general object recognition approaches to derive geometric primitives to form the building models.

This study aims to improve automatic BIM reconstruction in HD urban areas by proposing a reconstruction method called multi-Source recTification of gEometric Primitives (mSTEP). mSTEP harnesses the data from multiple sources and makes use of architectural features (*e.g.* parallels and symmetries) to reduce the noisy data and fine-tune the geometric primitives to reconstruct LoD2 BIMs automatically. The data employed in this study comes from the Hong Kong governmental agencies, comprising digital topographic map and light detection and ranging (LiDAR) point cloud. Given the fact that such types of data are extensively available in many cities and districts around the world, mSTEP can be applied to reconstruct their BIMs/CIMs in an efficient manner.

The organization of the paper is as follows: Section 2 reviews the state-of-the-art studies on BIM reconstruction. Section 3 describes the overall research progress, the subject area and characteristics of the corresponding topographic map and LiDAR point clouds. Section 4 details the BIM reconstruction method – mSTEP. Section 5 provides a comprehensive discussion of the evaluation results, discusses the parameter configuration of mSTEP, and shows the compatibility of mSTEP with a denser point cloud. Section 6 concludes with a summary and highlights future research directions.

2. Literature Review

Previous studies on the generation of BIMs in the urban environment can be viewed from two different perspectives: (1) The raw data used for BIM reconstruction; and (2) the methods employed in processing the data. While the two perspectives are related, the discussion deals with each perspective separately for the sake of clarity.

2.1 Original datasets

Aerial and satellite images are typical data sources for large-scale BIM reconstruction. Spaceborne sensors like IKONOS, QuickBird, and GeoEye-1 have provided 1m-resolution satellite images for 3D building reconstruction (Lafarge *et al.* 2008; Poli *et al.* 2015). Aerial image resolution can be even higher than that of satellite images, in some cases, reaching decimeter accuracy. Owing to their high image resolution as well as the widespread use of unmanned aerial vehicles (UAVs), the uses of aerial images to create 3D models of individual buildings or even to reconstruct the entire urban scenes are increasing (Li *et al.* 2016).

LiDAR point clouds have also been widely used for BIM reconstruction. It typically utilizes laser light which is projected on surfaces and its reflected backscattering is captured for generating 3D point clouds. Heo *et al.* (2013) used LiDAR point clouds to develop the models of 29 buildings. Other studies including Sun and Salvaggio (2013), Xiong *et al.* (2014), and Yan *et al.* (2016) used airborne LiDAR point clouds to model a limited number of buildings with roofs of various shapes. With the availability of city-scale LiDAR point clouds, Poullis and You (2009) created simplified BIMs within a large city area.

Topographic maps, which describe urban objects in terms of geometry, land use, and other attributes, are another important data source for BIM reconstruction at city- or district-scale. In addition to the topographic maps produced by government agencies, recent years have seen the

emergence of open-access geographic datasets. For example, OpenStreetMap (OSM) – a prominent volunteered geographic information service – has been used for BIM reconstruction (Over *et al.* 2010). However, without official verification, the common problem of open-access geographic datasets is their completeness and accuracy.

The use of single-source data for BIM reconstruction, be it aerial images or LiDAR point clouds, is prevailing but still poses problems such as “noise” data caused by complex urban features and incomplete information (Cheng *et al.* 2011). These drawbacks have given rise to increased use of multi-source data for BIM reconstruction. A number of studies have confirmed that using multi-source data can overcome some of the problems associated with the use of single-source data (Rottensteiner and Jansa 2002; Alexandar *et al.* 2009; You and Lin 2011; Henn *et al.* 2013; Zhang *et al.* 2014; Zhu *et al.* 2015).

2.2 Data processing methods

Various data processing methods have been proposed for BIM/CIM reconstruction (Haala and Kada 2010; Musialski *et al.* 2013). Aerial or satellite images can be processed into digital elevation model (DEM) (Lafarge *et al.* 2008; Poli *et al.* 2015) from which building models can be extracted by applying height thresholds. With the further development of image matching, an alternative way is to generate colored point clouds from a number of aligned aerial images and then processed the generated point clouds into textured BIMs, which are formed by a large number of small geometric primitives (Singh *et al.* 2014). This method, however, requires careful selection of images and manual interpretation to adjust the building models is often needed. Li *et al.* (2016) also generated point clouds from images, and proposed an object-level point cloud segmentation and roof extraction. However, their method was only tested on buildings with flat roofs.

Processing LiDAR data starts with segmentation of the point clouds of individual buildings. This can generally be achieved using semantic segmentation approach (Lin *et al.* 2013), classification or clustering algorithms (Zhu *et al.* 2015; Cao *et al.* 2017) or the reflectance value captured by the LiDAR sensors (Sun and Salvaggio 2013). LiDAR point clouds can also be integrated with other datasets. For example, building footprints retrieved from a topographic map can provide a reference for segmenting the point clouds of buildings (Alexander *et al.* 2009; Ledoux and Meijers 2011). The segmentation of LiDAR point clouds can also be improved with aerial images that provide regions of homogeneous gray level or color

distribution (Rottensteiner and Jansa 2002). Once segmented, the point clouds are used to model the buildings with roofs and rooftop objects by various methods. A typical method is to decompose the roof shapes into simple pre-defined ones by 2D plans (Henn *et al.* 2013) or graph matching technique (Xiong *et al.* 2014), but the reconstruction may fail if the roof shape is not pre-defined in the model library. Connecting the extracted primitives to form the roof features is also widely-used due to its flexibility (Poullis and You 2009; Zhang *et al.* 2014; Yan *et al.* 2016). However, such kind of method is sensitive to noise (Goebbelsa and Pohle-Fröhlich 2016) and so far have only been used for specific roof forms.

Although it is difficult to directly compare all these reconstruction methods since they are developed under different context with their own emphasis, our review has revealed that existing data processing methods usually require much time for noise filtering and assume buildings with flat or other simplified roof structures. Those methods that can generate more differentiated building and roof structures require considerable manual interpretation for pre- or post-processing. Actually, architectural designs commonly exhibit some conventional features such as parallels, symmetries or other structural regularities, which are not accidental, but often the result of economical, manufacturing, functional, or aesthetic considerations (Mitra and Pauly 2008). Parallel and perpendicular features have been used as the constraints to segment the point cloud to extract planar segments that constitute approximate building roof structure (Dorninger and Pfeifer 2008, Sampath and Shan 2010). However, few studies have systematically applied architectural rules to reconstructing BIMs of densely-distributed buildings in large-scale urban areas. As will be demonstrated in this study, rules derived from architectural conventions can help reduce the noise in the collected data and improve the efficiency of the modeling method and the informativeness of the reconstructed models.

3. Research approach

3.1 Overview of the research process

Given the aim of this study, a design science research approach (Peppers *et al.* 2008) is adopted to develop an automatic and efficient BIM reconstruction method. Design science focuses on not only understanding problems, but also developing methods or artifacts with the explicit intention of improving human performance (Van Aken 2005). A diagrammatic illustration of the research process is presented in Figure 1.

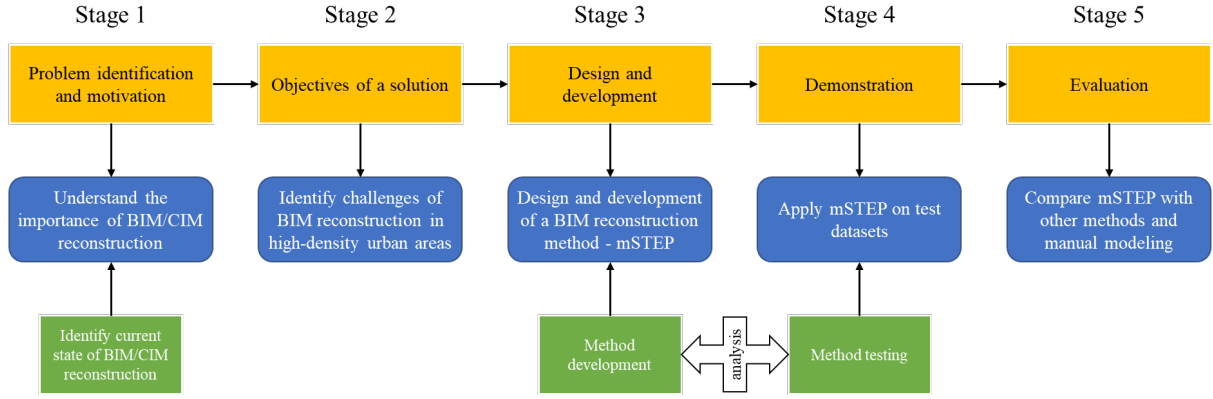


Figure 1 Research process

By identifying the challenges of BIM reconstruction in high-density urban areas, multi-Source recTification of gEometric Primitives (mSTEP) was proposed, which takes the topographic map, point clouds, and architectural conventions as inputs and generates BIMs with detailed rooftop structures and objects identified. A 2km×2km area in northwestern Hong Kong Island, containing 1,361 blocks of densely-distributed buildings of varying heights and shapes, was selected as the subject area since all identified challenges of BIM reconstruction exist in this area: The buildings are surrounded by urban features like trees on hills and slopes, commercial signs and power lines, which create noise in the data captured for BIM reconstruction; The narrow gaps between buildings also cause severe occlusions in the collected data. In combination, these factors present difficulties for segmentation, refinement and other BIM reconstruction processes. After applying mSTEP on test datasets, the generated BIMs were compared with results from another two reconstruction methods (*i.e.* methods described in Javanmardi et al. [2015] and Wu et al. [2017]) and manual modeling for evaluation.

3.2 Test datasets

The topographic map used in this study was purchased from the Lands Department (LD) of HKSAR. It is in Geodatabase (GDB) format with a scale of 1:1000. The Hong Kong 1980 Grid Coordinates provides the latitude and longitude of the map, and heights are in meters above the Hong Kong Principal Datum. The topographic map contains feature datasets including *buildings, land cover, transportation*, etc. As shown in Figure 2, the buildings in the selected region are shown in green with their boundaries in black. The map also contains data on building ID, shape, shape area, type of building block, base level, roof level, and data source. A preliminary analysis of the base and roof levels found that the datasets in the topographic map are collected from various sources such as building plans, photogrammetry, and

topographic survey. Data for the buildings was last updated in the period 1 July 2014 to 27 April 2016.

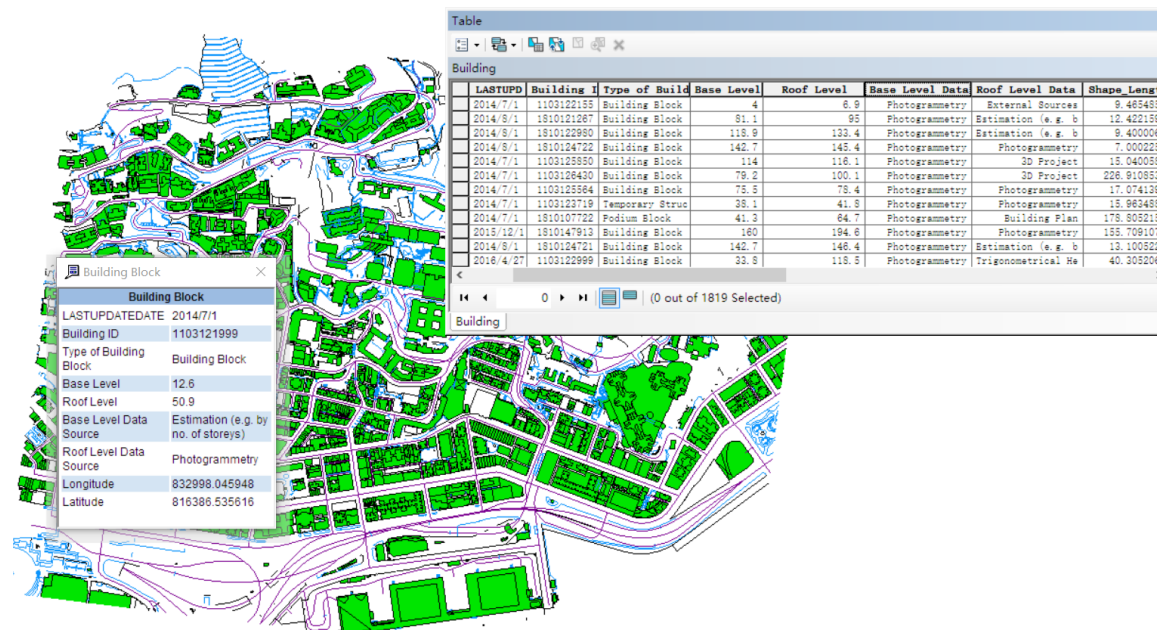


Figure 2 Data of the topographic map of the subject area

The LiDAR point clouds used in this study was provided by the Civil Engineering and Development Department (CEDD) of HKSAR. The data, comprising buildings, roads, and many other urban features, was collected between 1 December 2010 and 8 January 2011 by the CEDD by hiring an airborne LiDAR surveying company. In the original dataset, the point density is about 4 points/m². Points classified according to American Society for Photogrammetry and Remote Sensing (ASPRS) laser (LAS) format specification 1.1 (ASPRS 2005) are shown in different colors (see Figure 3). The classification codes represent the type of object that has reflected the laser pulse.

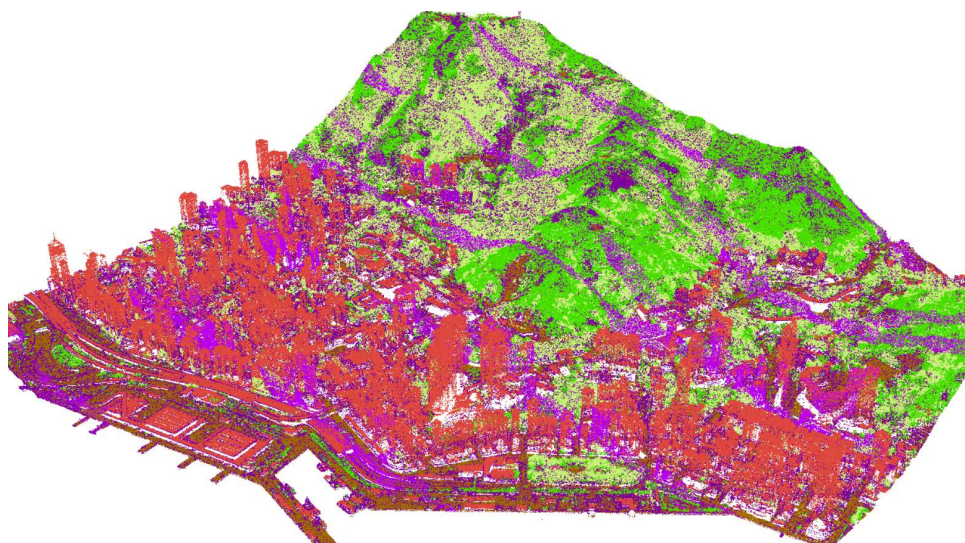


Figure 3 An illustration of the LiDAR point clouds

4. BIM reconstruction method

The main purpose of the proposed method — multi-Source recTification of gEometric Primitives (mSTEP) — is to enable automatic and efficient BIM reconstruction. The overall procedure of mSTEP is shown in Figure 4, which consists of four main phases. In this section, each of the four phases of mSTEP is introduced in details.

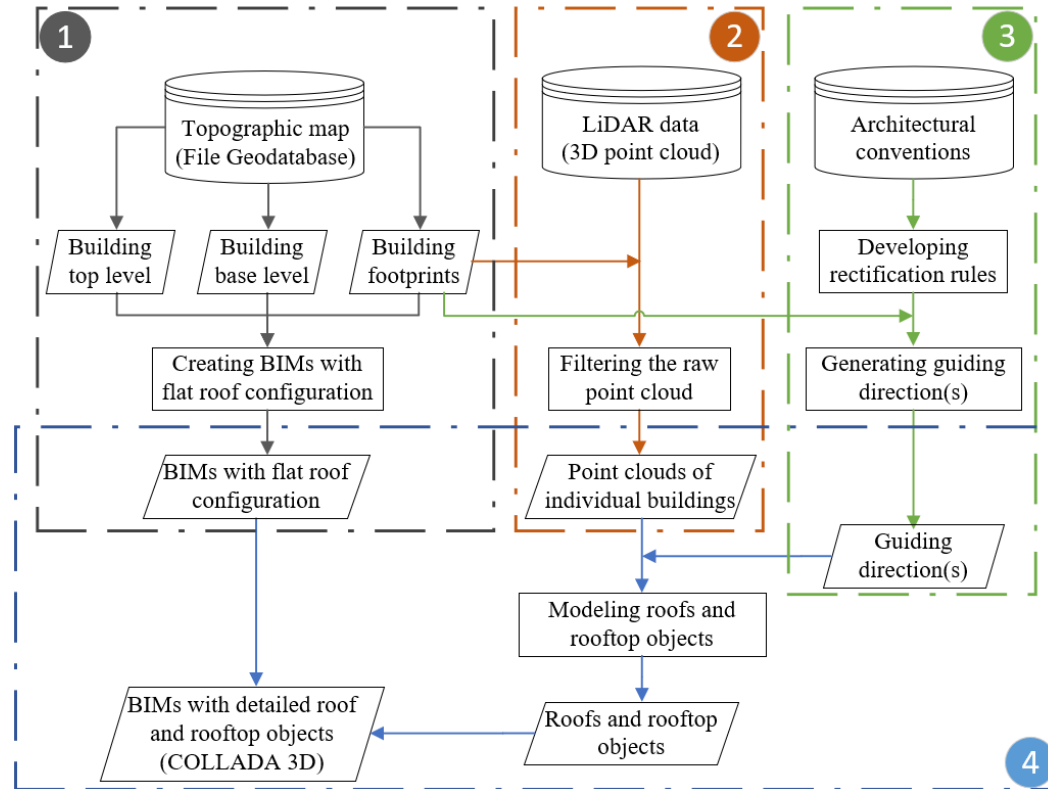


Figure 4 Overall procedure of mSTEP

4.1 Reconstructing LoD1 BIMs from topographic map

In the first phase, data in the topographic map is filtered to retrieve the data of building footprint, base level, and top level. By vertically stretching the footprint of each building according to the base level and top level of that building, the LoD1 BIM with flat roof configuration can be created (see Figure 5).

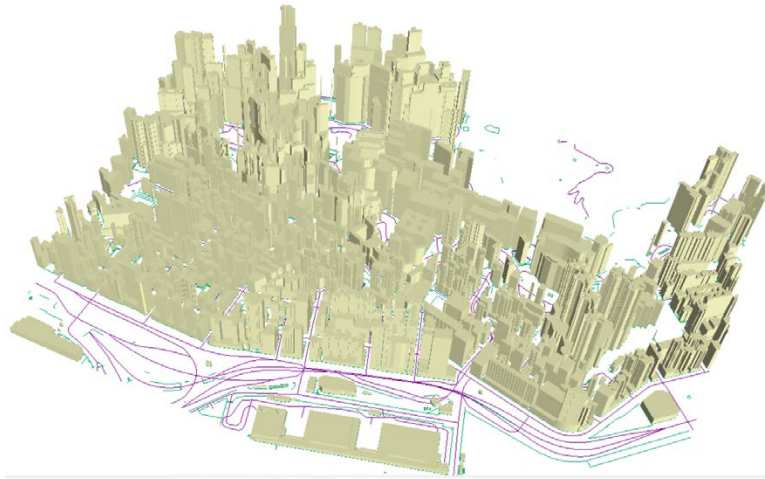


Figure 5 An illustration of created LoD1 BIMs

4.2 Filtering the LiDAR point clouds

The LiDAR point clouds is first filtered in *ESRI ArcScene* by using the classification codes to separate building point clouds from those of trees, terrain, and other features (ESRI 2016). However, it was found that many points of building structures were unclassified (see the circled area in Figure 6). Therefore, points classified as either “building” or “unclassified” were thus kept for further rectifications and other points were removed. Then, the point cloud of individual buildings was obtained by segmentation, a process accelerated through the use of building footprints contained in the topographic map. After converting the LiDAR point clouds and topographic map in the same coordinate system, points with XY-coordinates falling into the area zoned by a building footprint was segmented to that building.

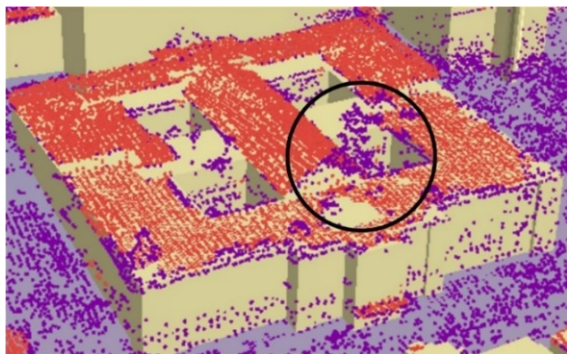


Figure 6 An example of unclassified points in the raw LiDAR point clouds

4.3 Developing object rectification rules from conventional architectural features

Architectural conventions refer to the domain knowledge applied in the architectural design, such as geometrical or physical features (*e.g.* flatness, parallels, and symmetries) of building objects and their spatial relationships (Cantzler 2003). Some of the conventions can be obtained

from ordinances or standards, while others can be originated from general observation in real-world situations. In this study, two object rectification rules are developed based on very simple architectural conventions to ensure “structural regularity”: (1) the top surface of rooftop objects are either in parallel with the horizontal plane or with a considerable angle of dip; and (2) the rooftop objects are normally in parallel with the outer edge of roof.

Both rules should be satisfied when rectifying the geometric primitives detected from the segmented LiDAR point clouds to form roofs and rooftop objects. An illustration of rectification by the first rule is presented in Figure 7(a). The rectangle in blue is the top surface of a rooftop object, which has a very small angle β of dip to the horizontal plane (*i.e.* the roof). Therefore, this detected primitive is against the first rule, and should be rotated to be the rectangle in gray, which is in parallel with the horizontal plane. An illustration of rectification by the second architectural rule is shown in Figure 7(b). The rectangle in dashed line is not in parallel with the outer edge of the roof, but has a deviation of angle α . This is rare in architectural conventions, therefore, it should be rotated to be the rectangle in gray.

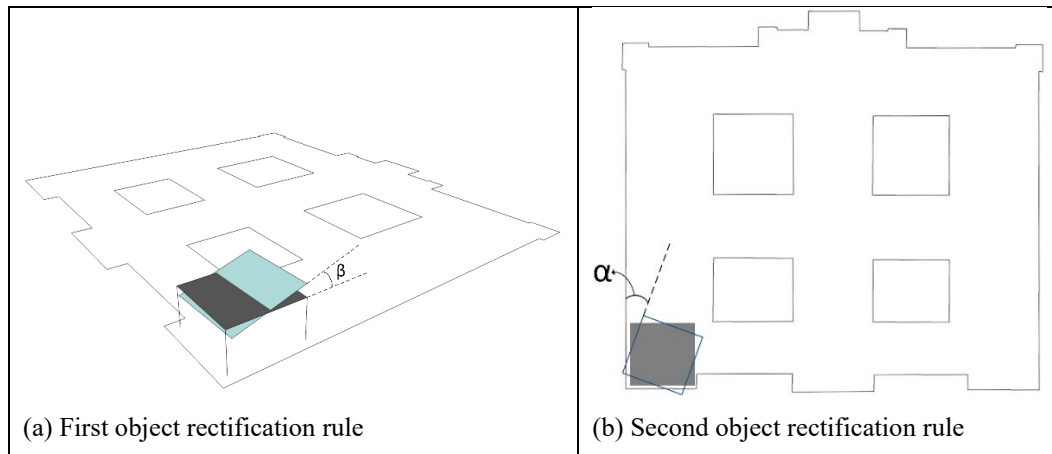


Figure 7 An illustration of the two rules of rectification

In order to enable automatic application of these two rules, especially the second one, guiding directions were derived from the building footprints since the outer edge of the roof and building footprint usually have the same shape, unless it is an irregular-shaped building. As can be seen in Figures 8(a) and (b), for simple, regular-shaped building footprint, its centerline provide the guiding direction for the rooftop object to be in parallel with, while for irregular-shaped building footprint, the centerlines of its top 25% longest lines will provide guiding directions for the computer to check whether the rooftop object is in parallel with at least one of the directions.

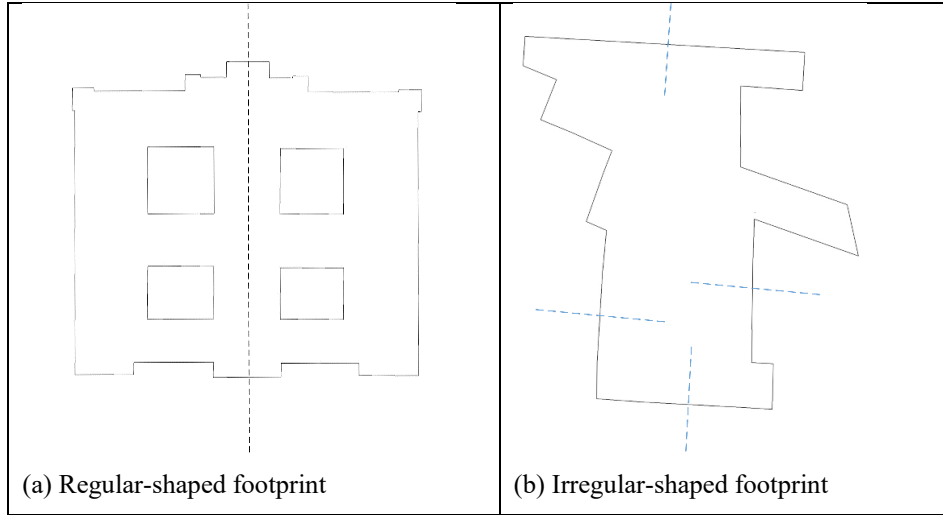


Figure 8 An illustration of deriving guiding direction(s) from building footprints

4.4 Reconstructing LoD2 BIM by using object rectification rules

In the last phase of mSTEP, LoD2 BIM is developed by using the two object rectification rules. The pseudo code of this process is shown in Figure 9. Given a target building, its LoD1 model is inherited from the topographic map (Line 6). A variant of RANSAC (Fischler and Bolles 1981; Schnabel *et al.* 2007) is adopted for detecting geometric primitives from LiDAR point cloud of the building rooftop (Lines 7-8). The application of RANSAC requires a set of parameters to be determined (see Table 1). Different values of these parameters have been tested in order to find the optimal parameter set regarding the LiDAR point clouds to be processed. It is decided to set *minimum number of support points* to 10, *maximum distance to primitive* to 0.02m, and *sampling resolution* to 1.0. *Maximum normal deviation* and *overlooking probability*, are set to 25° and 1.0×10^{-6} respectively. More details regarding the parameters configuration are provided in Section 5.2.

Then, the detected geometric primitives are rectified to form the building roofs and rooftop objects. A tolerance level (ϵ), which is set to 0.05π , is used to determine whether one primitive needs rectification or not. The detected geometric primitives of roofs and rooftop objects will be rectified by the horizontal plane (Lines 9-13) and the guiding directions (Lines 14-21). After rectification, the volumetric models of roofs and rooftop objects can be created by projection to the top level of individual buildings, and will be integrated with the LoD1 BIMs created in the first phase to enrich them into LoD2 ones that have differentiated roof structures with higher completeness and accuracy (Lines 22-24).

```

2   input: a set of building exterior data sources ( $S$ ) of a building, including data in topographic map and
        LiDAR point clouds,
3       five parameters ( $param$ ) of RANSAC,
4       a tolerance level ( $\varepsilon$ ) for orientation rectification (default value of  $0.05\pi$ )
5   output: an LoD2 building model ( $M$ ) with detailed roof and rooftop objects
6    $M \leftarrow$  a LoD1 model from topographic map ( $S$ )           //referring to subsection 4.1
7    $r \leftarrow$  filter point cloud of rooftops ( $S$ );           //referring to subsection 4.2
8    $P \leftarrow$  RANSAC ( $r, param$ );                           //detecting geometric primitives
9   loop for each  $p$  in  $P$                                      //for each detected geometric primitive
10       $\alpha \leftarrow$  heading of normal ( $p$ );  $\beta \leftarrow$  dip of plane ( $p$ ); // for  $\alpha$  and  $\beta$  referring to Figure 7
11      if  $|\beta| < \varepsilon$  or  $|\pi - \beta| < \varepsilon$              //if  $\beta$  is close to the horizontal plane
12           $\beta \leftarrow 0$                                      //rectify w.r.t. the horizontal plane (as shown in Figure 7[a])
13      end if
14       $A \leftarrow$  derived guiding directions;
15      loop for each  $\alpha^*$  in  $A$                                //for each direction  $\alpha^*$ 
16          loop for  $q = -2$  to  $2$                              //for each quadrant
17              if  $|\alpha - \alpha^* + q \times \pi / 2| < \varepsilon$  //if  $\alpha$  is close to  $\alpha^*$ 
18                   $\alpha \leftarrow \alpha^* - q \times \pi / 2$  //rectify w.r.t. the direction  $\alpha^*$  (as shown in Figure 7[b])
19              end if
20          end loop
21      end loop
22      if  $\alpha, \beta$  meets the two object rectification rules
23           $M \leftarrow M \cup \text{update and 3D projection}(p, \alpha, \beta)$  //enrich LoD1 BIM with roof and rooftop objects
24      end if
25  end loop
26  return  $M$ 

```

Figure 9 Pseudo code of the multi-source rectification

Table 1 Descriptions of the RANSAC parameters

Parameter	Description
minimum number of support points	The minimum number of points required to identify a geometry. A larger <i>minimum support points</i> means a more rigorous geometry detection process.
maximum distance to primitive	The maximum distance of an inlier point to a geometry.
sampling resolution	The parameter determines the sample rate of neighboring points
maximum normal deviation	The difference between the normal at a point and the normal of a geometry at the closest project of that point onto that geometry.
overlooking probability	The parameter controls the population size of the primitive candidates.

A demonstration of multi-source rectification is shown in Figure 10. At the beginning, geometric primitives are detected from LiDAR point clouds (see Figure 10[a]) by RANSAC, but the detected geometric primitives may not be corrected from an architectural point of view. For instance, in Figure 10(b), the rectangle marked in red circle conjuncts to the roof surface at an angle. Then, the detected primitives are rectified according to the horizontal plane and the guiding direction(s). After that, the rectified primitives will be projected to create volumetric models of roofs and rooftop objects (see Figure 10[c]).

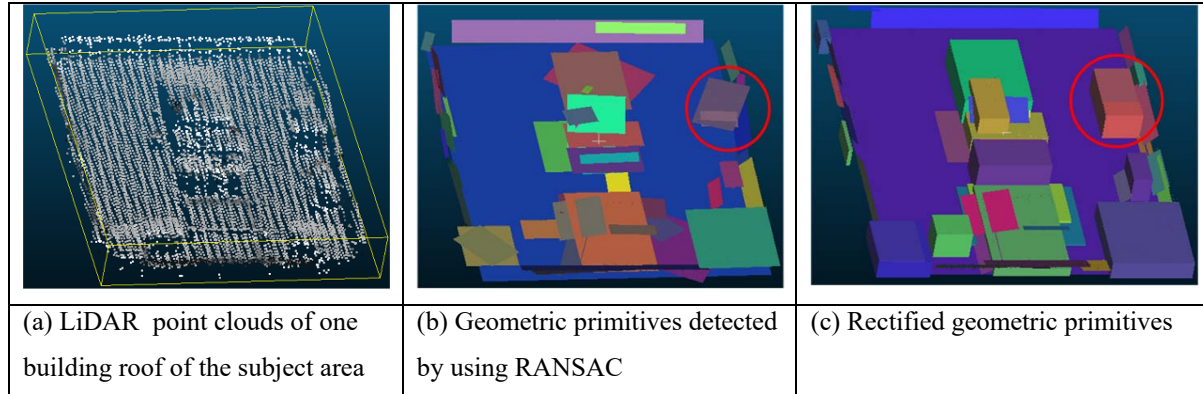


Figure 10 A demonstration of the multi-source rectification

5. Evaluation

5.1 Overall results

In this study, the first phase of mSTEP is performed in *ESRI ArcScene*, and the remaining three phases are automatically performed by using a plug-in of *CloudComapre* which is tailor-programmed in C++ by the authors. A screenshot of the plug-in is shown in Figure 11. The computation environment was a personal notebook with 2.6GHz Quad-core CPU, 16 GB RAM, and a 64-bit Microsoft Windows 10 operating system. Applying mSTEP, the automatic generation of BIMs in the subject area took 319.7 seconds. 81.9% of the 1,361 buildings were successfully modeled. Among the remainder, 113 buildings do not have either the base level or the roof level in the topographic map, and 134 buildings lacked points in the LiDAR dataset for modeling of the roofs and the rooftop objects.

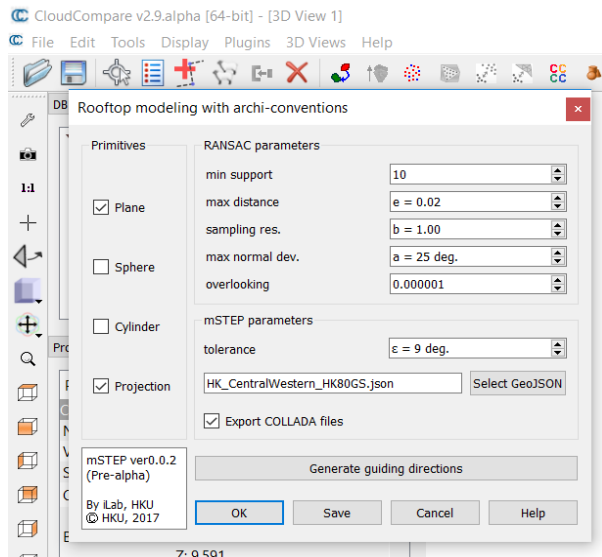
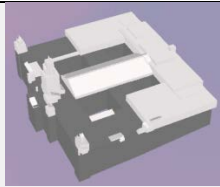





Figure 11 The screenshot of the developed *CloudCompare* plug-in

Some examples of the reconstructed models are shown in Figure 12. Among the buildings shown include a building on a university campus (*ID: 11**374*), Edwardian Baroque in style with a central clock tower and several turrets; a residential building with a pyramid-shaped roof and many rooftop objects (*ID: 11**486*); a wholesale food market with a strip-shaped roof and several box-shaped air conditioners (*ID: 11**535*); and a residential building (*ID: 11**845*) with flat roof and cuboid-shaped rooftop objects. Other building models shown in Figure 12 also have their roof and rooftop objects in the correct shapes constituted without the need for manual post-modifications. By manually checking the 3D building models and the actual buildings, it can be seen that the models reach the LoD2 that possess more detailed information than simple “boxes”. It can also be seen that the models are in an acceptable standard of accuracy.

Building ID in the topographic map	Reconstructed model (colors are for distinguishing only)	Photo (collected from the Internet or taken by the authors)
11**374		
11**486		

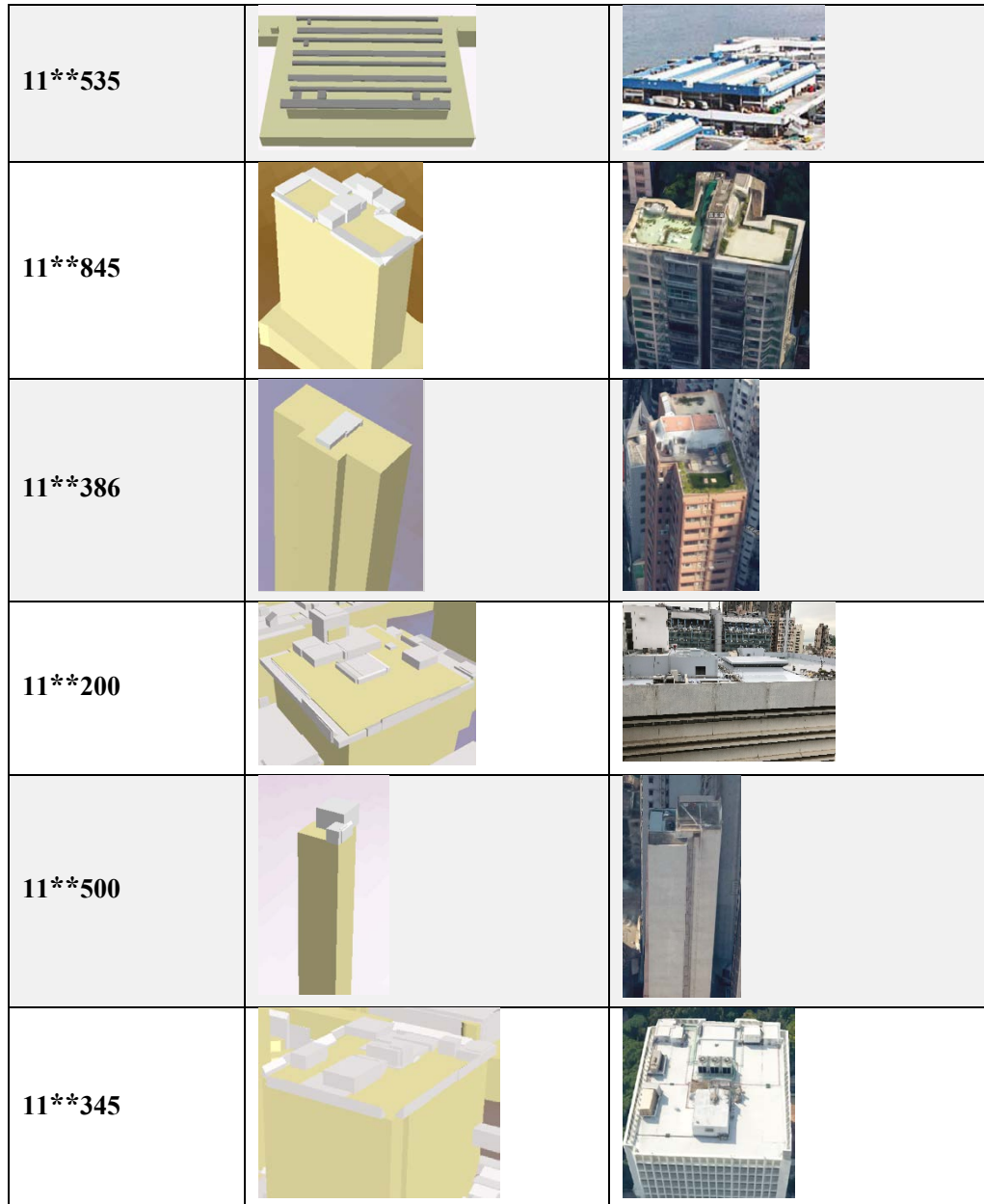


Figure 12 An illustration of the reconstructed models and actual buildings

5.1.1 Efficiency assessment

To assess the efficiency of reconstruction, the time spent on reconstructing buildings by using mSTEP was compared with the time required for manual modeling. In *SketchUp*, two human modelers, who have over four years' experience in architectural drawing, created LoD2 BIMs based on base and roof levels from the topographic map and the segmented LiDAR point clouds. They began modeling at the same time and alerted the researchers once they finished each of the nine models so that the time they spent on modeling each building was recorded. In addition, mSTEP was compared with: (1) a concave hull and Hough transform based reconstruction method (take LiDAR point cloud and topographic map as inputs) introduced in Javanmardi et

al. (2015); and (2) a bipartite graphic matching-based reconstruction method introduced in Wu et al. (2017). The two reconstruction methods were selected for comparison due to two reasons. First, all the three methods share the same vision of enhancing 3D model reconstruction by taking advantage of architectural conventions and graph theory. The other reason was that their input point clouds were all airborne LiDAR data of HD urban areas. The comparison was based on three commonly-adopted metrics, including (1) *reconstruction time*; (2) *percentage of points that are segmented to support the detection of geometric primitives*; and (3) *root mean square error (RMSE) of the distances of points to their corresponding primitives*. The assessment results on nine randomly-selected buildings are presented in Table 2.

Table 2 Assessment results

No.	Number of points	mSTEP			Javanmardi et al. (2015) [†]			Wu et al. (2017) [‡]			Manual
		Time (s)	Segmented (%) [#]	RMSE (m) [*]	Time (s)	Segmented (%) [#]	RMSE (m) [*]	Time (s)	Segmented (%) [#]	RMSE (m) [*]	Time (In average; s)
1	270	0.03	75.2	0.114	0.02	63.1	0.119	0.01	88.3	0.341	266.65
2	372	0.03	77.7	0.048	0.01	58.7	0.157	0.01	60.4	0.223	171.23
3	620	0.40	87.6	0.065	0.02	84.7	0.098	0.01	78.8	0.370	94.33
4	2,491	0.16	48.6	0.196	0.05	31.6	0.199	0.01	99.8	0.315	2,486.75
5	2,682	0.09	90.0	0.057	0.03	60.2	0.049	0.01	89.6	0.251	515.65
6	7,212	0.23	91.1	0.067	0.04	26.4	0.067	0.01	90.4	0.280	597.92
7	8,987	0.26	85.1	0.065	0.09	18.8	0.097	0.01	100.0	0.257	1,386.16
8	24,878	2.23	86.3	0.068	0.13	66.2	0.163	0.02	99.1	0.340	2,498.84
9	29,506	0.47	90.1	0.088	0.21	71.1	0.230	0.02	99.9	0.291	701.43

[†]: The parameter β of Javanmardi et al. (2015)'s method was set to 0.5m as the average point distance;

[‡]: The two parameters, i.e., variable n and contour interval d_i , were set as 250 and 0.5m based on Wu et al. (2017)'s experimental results.

[#]: Percentage of points that are segmented to support the detection of geometric primitives.

^{*}: Root mean square error of the distances of segmented points to their corresponding primitives.

The results in Table 2 showed that mSTEP achieved a competitive performance. Specifically, both mSTEP and Javanmardi et al. (2015)'s method reconstructed accurate geometric primitives for segmenting the point clouds. The proposed mSTEP segmented more points than Javanmardi et al. (2015)'s to support the detection of geometric primitives and reconstruct BIMs with less RMSE. In contrast, Wu et al. (2017)'s method achieved a fast reconstruction with a high-level of segmentation; yet at a significant cost of error (see the level of RMSE). The results confirmed that mSTEP could overcome the three identified challenges in BIM reconstruction in HD urban areas, i.e., much noise in measurement data, difficulties in segmenting data of densely-distributed buildings, and high computational complexity. With

the help of mSTEP, the efficiency of BIM reconstruction in HD urban areas can be considerably improved.

Nevertheless, there seems no convincing way to measure the exact accuracy of the reconstructed BIMs scientifically due to the lack of ground truth (Poullis and You 2009; Sun and Salvaggio 2013). It is far from an effective measurement to reflect the resemblance between the generated BIMs and the “as-is” condition. Neither can the model accuracy be measured using a single index, such as the physical volume. A BIM professional, with expertise and insights, can also tell whether the accuracy of a reconstructed 3D model is “acceptable” or not. The issue of measurement standard is left for further studies.

5.1.2 Identified problems

During application of mSTEP, it was found that the modeling outcomes can be affected by the accuracy of data used, including the building footprints and heights in the topographic map, and the LiDAR point clouds. Regarding the topographic map used in this study, some building footprints were inaccurate and some heights were generated by estimation. This affected the quality and accuracy of the retrieved guiding directions and, in turn, the accuracy of geometric primitives detected from the point clouds.

Regarding the accuracy of the LiDAR point clouds, this is adversely affected by missing points and interference caused by densely-distributed buildings, city features, and the like. mSTEP can address interference, but not the problem of missing data. In this study, three factors resulted in missing data. Firstly, the LiDAR scan pulse typically does not provide a detectable return from transparent materials such as glass. Therefore, the points for roofs and rooftop objects made of such materials were missing and thus could not be used for BIM reconstruction. Secondly, the density of the point cloud was 4 points/m². This may not be sufficient to capture data on certain rooftop objects, such as parapet walls that are relatively thin in the horizontal dimension. Thirdly, the LiDAR point clouds, collected from 2010 and 2011, was not up-to-date.

5.2 Parameter configuration of mSTEP

A set of tests was performed on the parameter configuration of mSTEP. The purpose is to identify the parameters that can significantly impact the modeling outcomes measured by the *average number of detected geometric primitives*. This indicator is chosen because it measures

the primitives generated from the LiDAR point clouds to form the roof and rooftop objects. Generally, the larger value the indicator, the more details the roof and rooftop objects have been reconstructed by mSTEP. However, excessive primitives detected are also undesirable since they are often caused by a single rooftop object being separated into several small pieces (e.g. a pipe separated into different trunks), which actually decrease the accuracy of reconstruction.

The parameters to be tested include the *tolerance level* and the five RANSAC parameters in terms of (a) *minimum number of support points*, (b) *maximum normal deviation*, (c) *maximum distance to primitive*, (d) *sampling resolution*, and (e) *overlook probability*. The test subject is the LiDAR point clouds of a randomly-selected building, which has an ID 11**200 in Figure 12. The tests aim at evaluating the sensitivity of each parameter, therefore when performing the testing one parameter, other five parameters are controlled, *i.e.* remaining unchanged. In the single factor sensitivity analysis, for each parameter, the tests were replicated for 100 times to get the statistic values at 5th and the 95th percentiles. The results of all tests are shown in Figure 13. In each of the six sub-figures, the Y-axis on the left denote the number of geometric primitives detected by mSTEP, the X-axis denotes the value of the tested parameter. The box chart shows the average values, and the 5th and the 95th percentiles of the indicator. The curve depicted in each sub-figure illustrates the trend of value changes of the indicator as reflection to the value change of the parameter under evaluation.

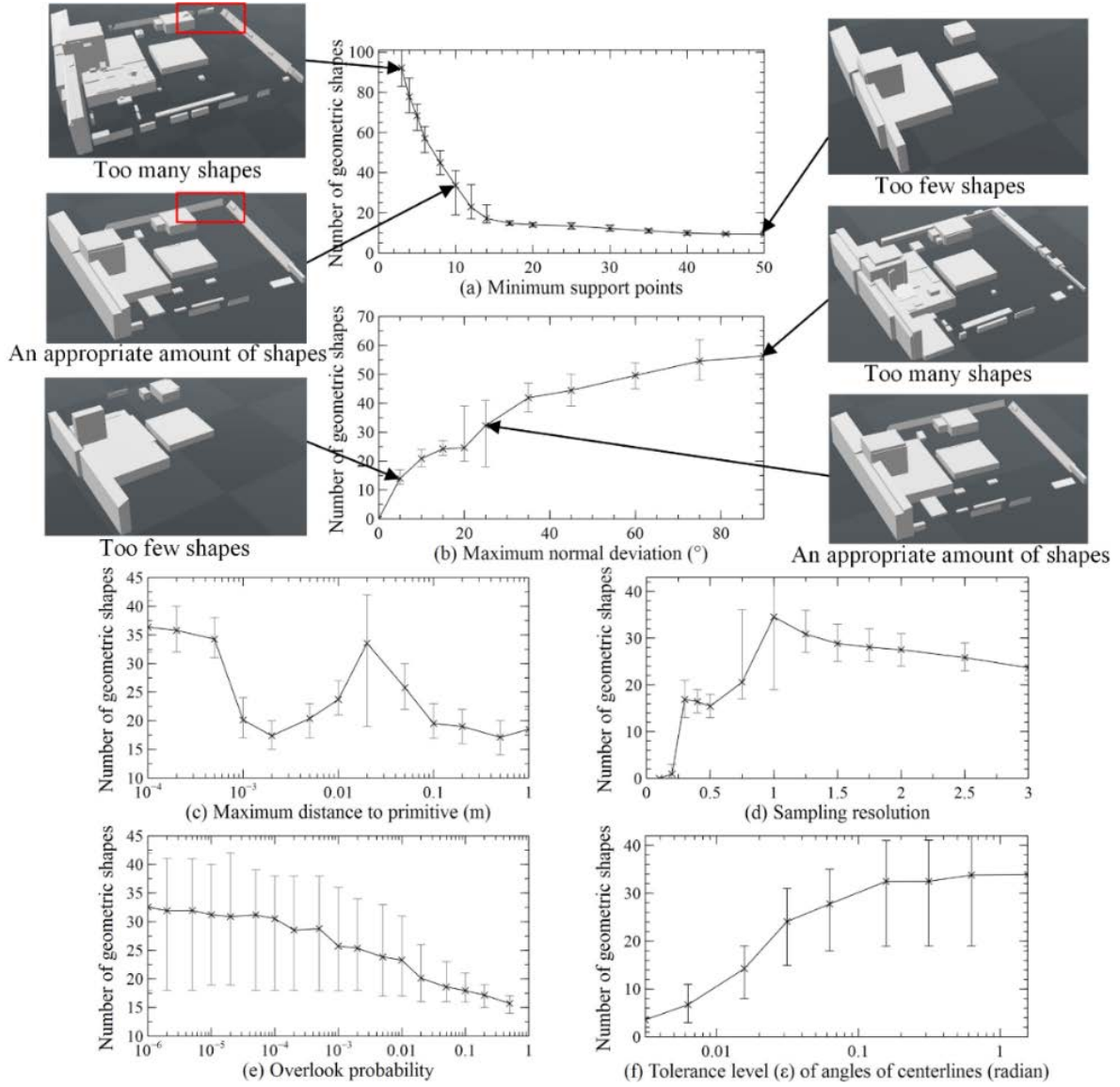


Figure 13 Testing results of parameter configuration of mSTEP

Based on the results shown in Figure 13, it can be confirmed that *minimum number of support points* and *maximum normal deviation* are the two parameters that have the most significant impact on the indicator of *average number of detected geometric primitives* since the curves shown in Figure 13(a) and (b) cover a much wider range in Y-axis than the curves in the other four figures. Particularly in Figure 13(a), when *minimum number of support points* increase from 3 to 10, the indicator decreases steeply from 95 to 33.6. Once *minimum number of support points* exceed 10, the indicator will continuously decrease, at a slower pace, to 9. From the three outputs of mSTEP when *minimum number of support points* equal to 3, 10 and 50 respectively, it can be seen that some of the rooftop objects such as the parapet wall are divided into small pieces (see the comparison between the two parts marked in red rectangle of Figure

13[a]). When *minimum number of support points* is set to 3, too many primitives are detected. By contrast, when *minimum number of support points* is set to 50, many details of rooftop objects are missing. Setting *minimum number of support points* to 10 can generate an appropriate output. In Figure 13(b), when *maximum normal deviation* increases from 0° to 90° , the *average number of detected geometric primitives* increases from 0 to 55.4. Similar to the evaluation on *minimum support points*, three outputs when *maximum normal deviation* equals to 5° , 25° , and 90° are presented, from which, it is found that setting *maximum normal deviation* to 5° and 90° lead to too few and too many detected primitives respectively. When *maximum normal deviation* equals 25° , an appropriate amount of primitives can be detected.

For the remaining four parameters, the impact of *maximum distance to primitive* on the indicator is relatively complex. As it increases from $1.0 \times 10^{-4}\text{m}$ to 1.0m , the *average number of detected geometric primitives* fluctuates (see Figure 13[c]). It seems that setting *maximum distance to primitive* to either $1.0 \times 10^{-4}\text{m}$ or 0.02m can deliver similar outputs in terms of quantity, but it is found that when *maximum distance to primitive* equals to $1.0 \times 10^{-4}\text{m}$, most of the detected primitives are too small, which shows a lack of accuracy. Therefore, 0.02m is the more appropriate value for *maximum distance to primitive*. Additionally, when *tolerance level* increases from 0.001π to 0.5π , the *average number of detected geometric primitives* increases from 3.58 to 33.91. Such impact, however, becomes negligible after *tolerance level* reaches 0.05π (see Figure 13[f]). For *sampling resolution*, when it is either less than 1.0 or large than 1.25, the *average number of detected geometric primitives* will become less than 30, which decreases the accuracy of the reconstructed roof and rooftop objects (see Figure 13[d]). Finally, for *overlook probability*, its overall influence is less significant compared with the other five parameters (see Figure 13[e]). Its values between 1.0×10^{-6} and 5×10^{-5} can detect an appropriate amount of primitives, but the best output is identified when setting *overlook probability* to 1.0×10^{-6} .

5.3 Implementing mSTEP on dense point cloud

The density of LiDAR point clouds used to reconstruct buildings in the subject areas is 4 points/ m^2 . With the improvement in sensing devices, the cost of data acquisition is expected to continuously decrease and denser point clouds will become available. Therefore, it is necessary to test the applicability of mSTEP to dense point clouds. Since few buildings in the subject area have publicly available dense point cloud, a building at the main campus of the University of Hong Kong in Hong Kong Island is selected for the test.

The dense point cloud of the selected building contains 482,404 points in total, which is obtained by using SfM to process 200 photos taken by a UAV (see Figure 14[a]). Details about SfM for processing images into point cloud can be found in Jancosek and Pajdla (2011). When applying mSTEP to this dense point cloud, one parameter, i.e. *minimum number of support points*, is changed from 10 to 30 in order to cope with the point density, while other five parameters remain unchanged. The rooftop model is developed in 1.41s with 475 geometric primitives detected (see Figure 14[b]). In doing so, mSTEP is proved to be capable of reconstructing BIMs from a denser point cloud. A conclusion thus can be drawn that mSTEP is applicable to both sparse point clouds (e.g. 4 points/m²) and dense point clouds for BIM reconstruction. This suggests mSTEP can be applied to 3D building reconstruction in many other cities or districts, which possess point clouds of various densities.

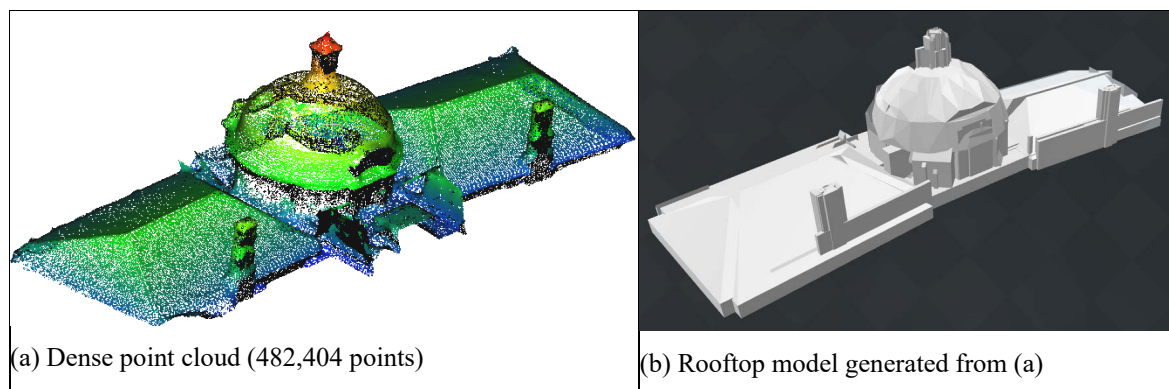


Figure 14 An illustration of applying mSTEP to a dense point cloud

6. Conclusions

The challenges of automatic reconstruction of building information models (BIMs)/city information models (CIMs) in high-density (HD) urban areas are predominately twofold: (a) the complex topographic conditions and noisy data, and (b) the heavy computational complexity when the task is at an urban scale. This paper took the challenges by developing an improved method — multi-Source recTification of gEometric Primitives (mSTEP) — for automatic BIM reconstruction in complex urban areas. mSTEP comprises of several interconnected steps to make good use of multi-source data including light detection and ranging (LiDAR) point clouds, and topographic maps. The method has been validated through a series of rigorous tests, and the results show that mSTEP is an efficient method to reconstruct informative BIMs by significantly improving the level of automation and decreasing the computation time.

Of particular originality of this research is augmenting the multi-source data with some simple architectural conventions, which can effectively tackle the challenges of automatic BIM/CIM reconstruction. Another original contribution made by this study is the optimal parameter configuration of mSTEP, which is derived from a series of sensitivity analyses of the parameters' impacts on the accuracy of the reconstructed models. As the paper shows, mSTEP can be applied to both sparse and dense point clouds. The research is thus of profound significance; It can help other cities or districts, which have possessed such “common” datasets as topographic map and LiDAR point clouds, to produce their own BIMs/CIMs to support their smart city programs.

Future research will be conducted in mainly three aspects. Firstly, the two object rectification rules used in the current version of mSTEP might be too restrictive when dealing with atypical architectures. Improvements thus are desired to allow reconstruction of buildings with curved and irregular-shaped roofs and rooftop objects. Secondly, data from other sources, such as aerial images, will be integrated with the topographic map and LiDAR point clouds to increase the level of detail (*e.g.* texture) of the generated models. In this connection, other architectural conventions such as symmetries or repetitive patterns should be exploited to facilitate the BIM reconstruction processes.

Acknowledgement

This study is financially supported by HKU Seed Fund (201702159013) and RGC General Research Fund (17201717). The assistance of the Civil Engineering and Development Department (CEDD) of Hong Kong SAR in providing LiDAR point clouds for research purposes is much appreciated. The authors are particularly in debt to Prof. Kincho Law at Stanford University, who has spent his precious time to provide several rounds of comments on the paper as it was developed. The authors would like to thank all the editors and anonymous reviewers for their constructive comments.

References

- AECbytes (2016). City Information Modeling. Available at: <http://www.aecbytes.com/feature/2016/CityInformationModeling.html>, Accessed date: 6 January 2017.
- Alexander, C., Smith-Voysey, S., Jarvis, C., and Tansey, K. (2009). Integrating building footprints and LiDAR elevation data to classify roof structures and visualise buildings.

- Computers, Environment and Urban Systems, 33(4), 285-292. doi:10.1016/j.compenvurbsys.2009.01.009.
- ASPRS (American Society for Photogrammetry & Remote Sensing). (2005). LAS specification version 1.1. Available at: http://www.asprs.org/wp-content/uploads/2010/12/asprs_las_format_v11.pdf, Accessed date: 6 January 2017.
- Awrangjeb, M., Zhang, C., and Fraser, C. S. (2013). Automatic extraction of building roofs using LIDAR data and multispectral imagery. *ISPRS Journal of Photogrammetry and Remote Sensing*, 83, 1-18. doi:10.1016/j.isprsjprs.2013.05.006.
- Cantzler, H. (2003). Improving architectural 3D reconstruction by constrained modelling. Doctoral thesis, University of Edinburgh. Available at: <https://www.inf.ed.ac.uk/publications/thesis/online/IP030017.pdf>, Accessed date: 6 January 2017.
- Cao, R., Zhang, Y., Liu, X., and Zhao, Z. (2017). 3D building roof reconstruction from airborne LiDAR point clouds: a framework based on a spatial database. *International Journal of Geographical Information Science*, 31(7), 1359-1380. doi:10.1080/13658816.2017.1301456.
- Cheng, L., Gong, J., Li, M., and Liu, Y. (2011). 3D building model reconstruction from multi-view aerial imagery and lidar data. *Photogrammetric Engineering & Remote Sensing*, 77(2), 125-139. doi:10.14358/PERS.77.2.125.
- Choi, J. O., Chen, X. B., and Kim, T. W. (2017). Opportunities and challenges of modular methods in dense urban environment. *International Journal of Construction Management*, 1-13. doi:10.1080/15623599.2017.1382093.
- Dorninger, P., and Pfeifer, N. (2008). A comprehensive automated 3D approach for building extraction, reconstruction, and regularization from airborne laser scanning point clouds. *Sensors*, 8(11), 7323-7343. doi:10.3390/s8117323.
- ESRI (2016). Lidar point classification, Available at: <http://desktop.arcgis.com/en/arcmap/10.4/manage-data/las-dataset/lidar-point-classification.htm>, Accessed date: 15 January 2017.
- Fischler, M. A., and Bolles, R. C. (1981). Random sample consensus: a paradigm for model fitting with applications to image analysis and automated cartography. *Communications of the ACM*, 24(6), 381-395. doi:10.1145/358669.358692.
- Gilani, S. A. N., Awrangjeb, M., and Lu, G. (2016). An automatic building extraction and regularisation technique using LiDAR point cloud data and Orthoimage. *Remote Sensing*, 8(3), 258. doi:10.3390/rs8030258.

- Goebbelsa, S., and Pohle-Fröhlich, R. (2016). Roof reconstruction from airborne laser scanning data based on image processing methods. *ISPRS Annals of Photogrammetry, Remote Sensing and Spatial Information Sciences*, 407-414. doi:10.5194/isprs-annals-III-3-407-2016.
- Gröger, G., and Plümer, L. (2012). CityGML–Interoperable semantic 3D city models. *ISPRS Journal of Photogrammetry and Remote Sensing*, 71, 12-33. doi:10.1016/j.isprsjprs.2012.04.004.
- Haala, N., and Kada, M. (2010). An update on automatic 3D building reconstruction. *ISPRS Journal of Photogrammetry and Remote Sensing*, 65(6), 570-580. doi:10.1016/j.isprsjprs.2010.09.006.
- Habib, A. F., Zhai, R., and Kim, C. (2010). Generation of complex polyhedral building models by integrating stereo-aerial imagery and lidar data. *Photogrammetric Engineering & Remote Sensing*, 76(5), 609-623. doi:10.14358/PERS.76.5.609.
- Henn, A., Gröger, G., Stroh, V., and Plümer, L. (2013). Model driven reconstruction of roofs from sparse LIDAR point clouds. *ISPRS Journal of Photogrammetry and Remote Sensing*, 76, 17-29. doi:10.1016/j.isprsjprs.2012.11.004.
- Henricsson, O., and Baltsavias, E. (1997) 3-D Building Reconstruction with ARUBA: A Qualitative and Quantitative Evaluation. In: Gruen, A., Baltsavias, E.P., Henricsson, O. (eds) *Automatic Extraction of Man-Made Objects from Aerial and Space Images (II)*. Monte Verità (Proceedings of the Centro Stefano Franscini Ascona). Birkhäuser, Basel. doi:10.1007/978-3-0348-8906-3_7.
- Heo, J., Jeong, S., Park, H. K., Jung, J., Han, S., Hong, S., and Sohn, H. G. (2013). Productive high-complexity 3D city modeling with point clouds collected from terrestrial LiDAR. *Computers, Environment and Urban Systems*, 41, 26-38. doi:10.1016/j.compenvurbsys.2013.04.002.
- Jancosek, M., and Pajdla, T. (2011). Multi-view reconstruction preserving weakly-supported surfaces. In , 2011 IEEE Conference on Computer Vision and Pattern Recognition, pp. 3121-3128. IEEE. doi:10.1109/CVPR.2011.5995693.
- Javanmardi, M., Gu, Y., Javanmardi, E., Hsu, L. T., and Kamijo, S. (2015). 3D building map reconstruction in dense urban areas by integrating airborne laser point cloud with 2D boundary map. In 2015 IEEE International Conference on Vehicular Electronics and Safety, pp. 126-131. IEEE. doi:10.1109/ICVES.2015.7396906.
- Lafarge, F., Descombes, X., Zerubia, J., and Pierrot-Deseilligny, M. (2008). Automatic building extraction from DEMs using an object approach and application to the 3D-city

- modeling. *ISPRS Journal of Photogrammetry and Remote Sensing*, 63(3), 365-381. doi:10.1016/j.isprsjprs.2007.09.003.
- Ledoux, H., and Meijers, M. (2011). Topologically consistent 3D city models obtained by extrusion. *International Journal of Geographical Information Science*, 25(4), 557-574. doi:10.1080/13658811003623277.
- Li, X., Lv, Z., Hu, J., Zhang, B., Shi, L., and Feng, S. (2015). XEarth: A 3D GIS platform for managing massive city information. In *2015 IEEE International Conference on Computational Intelligence and Virtual Environments for Measurement Systems and Applications*, pp. 1-6. IEEE. doi:10.1109/CIVEMSA.2015.7158625.
- Li, M., Nan, L., Smith, N., and Wonka, P. (2016). Reconstructing building mass models from UAV images. *Computers & Graphics*, 54, 84-93. doi:10.1016/j.cag.2015.07.004.
- Lillesand, T., Kiefer, R. W., and Chipman, J. (2015). *Remote sensing and image interpretation*. John Wiley & Sons (ISBN-13: 978-1118343289).
- Lin, H., Gao, J., Zhou, Y., Lu, G., Ye, M., Zhang, C., Liu, L., and Yang, R. (2013). Semantic decomposition and reconstruction of residential scenes from LiDAR data. *ACM Transactions on Graphics*, 32(4), 66. doi:10.1145/2461912.2461969.
- Mitra, N. J., and Pauly, M. (2008). Symmetry for architectural design. In *Advances in Architectural Geometry*, 13-16. Available at: http://www0.cs.ucl.ac.uk/staff/n.mitra/research/archi_symm/paper_docs/archi_symm_agg_08.pdf, Accessed date: 6 January 2017.
- Musialski, P., Wonka, P., Aliaga, D. G., Wimmer, M., Gool, L. V., and Purgathofer, W. (2013). A survey of urban reconstruction. *Computer Graphics Forum*, 32(6), 146-177. doi:10.1111/cgf.12077.
- Open Geospatial Consortium (2012). *OGC City Geography Markup Language (CityGML) Encoding Standard*. Available at: <http://www.opengeospatial.org/standards/citygml>, Accessed date: 6 January 2017.
- Over, M., Schilling, A., Neubauer, S., and Zipf, A. (2010). Generating web-based 3D City Models from OpenStreetMap: The current situation in Germany. *Computers, Environment and Urban Systems*, 34(6), 496-507. doi:10.1016/j.compenvurbsys.2010.05.001.
- Peffer, K., Tuunanen, T., Rothenberger, M. A., and Chatterjee, S. (2007). A design science research methodology for information systems research. *Journal of Management Information Systems*, 24(3), 45-77. doi:10.2753/MIS0742-1222240302.

- Poli, D., Remondino, F., Angiuli, E., and Agugiaro, G. (2015). Radiometric and geometric evaluation of GeoEye-1, WorldView-2 and Pléiades-1A stereo images for 3D information extraction. *ISPRS Journal of Photogrammetry and Remote Sensing*, 100, 35-47. doi:10.1016/j.isprsjprs.2014.04.007.
- Poullis, C., and You, S. (2009). Automatic reconstruction of cities from remote sensor data. In 2009. IEEE Conference on Computer Vision and Pattern Recognition, pp. 2775-2782. IEEE. doi:10.1109/CVPR.2009.5206562.
- Rottensteiner, F., and Jansa, J. (2002). Automatic extraction of buildings from LIDAR data and aerial images. *International Archives of Photogrammetry Remote Sensing and Spatial Information Sciences*. Available at: <http://www.isprs.org/proceedings/XXXIV/part4/pdfpapers/204.pdf>, Accessed date: 6 January 2017.
- Sampath, A., and Shan, J. (2010). Segmentation and reconstruction of polyhedral building roofs from aerial lidar point clouds. *IEEE Transactions on Geoscience and Remote Sensing*, 48(3), 1554-1567. doi:10.1109/TGRS.2009.2030180.
- Schnabel, R., Wahl, R., and Klein, R. (2007). Efficient RANSAC for point-cloud shape detection. *Computer Graphics Forum*, 26(2), 214-226. doi:10.1111/j.1467-8659.2007.01016.x.
- Singh, S. P., Jain, K., and Mandla, V. R. (2014). A new approach towards image based virtual 3D city modeling by using close range photogrammetry. *ISPRS Annals of Photogrammetry, Remote Sensing and Spatial Information Sciences*, 2(5), 329. doi:10.5194/isprsannals-II-5-329-2014.
- Sun, S., and Salvaggio, C. (2013). Aerial 3D building detection and modeling from airborne LiDAR point clouds. *IEEE Journal of Selected Topics in Applied Earth Observations and Remote Sensing*, 6(3), 1440-1449. doi:10.1109/JSTARS.2013.2251457.
- Tang, P., Huber, D., Akinci, B., Lipman, R., and Lytle, A. (2010). Automatic reconstruction of as-built building information models from laser-scanned point clouds: A review of related techniques. *Automation in Construction*, 19(7), 829-843. doi:10.1016/j.autcon.2010.06.007.
- Van Aken, J. E. (2005). Management research as a design science: Articulating the research products of mode 2 knowledge production in management. *British Journal of Management*, 16(1), 19-36. doi:10.1111/j.1467-8551.2005.00437.x.

- Volk, R., Stengel, J., and Schultmann, F. (2014). Building Information Modeling (BIM) for existing buildings—Literature review and future needs. *Automation in Construction*, 38, 109-127. doi:10.1016/j.autcon.2013.10.023.
- Xiong, B., Elberink, S. O., and Vosselman, G. (2014). A graph edit dictionary for correcting errors in roof topology graphs reconstructed from point clouds. *ISPRS Journal of Photogrammetry and Remote Sensing*, 93, 227-242. doi:10.1016/j.isprsjprs.2014.01.007.
- Wu, B., Yu, B., Wu, Q., Yao, S., Zhao, F., Mao, W., and Wu, J. (2017). A graph-based approach for 3D building model reconstruction from airborne LIDAR point clouds. *Remote Sensing*, 9(1), 92. doi:10.3390/rs9010092.
- Xue, F., Chen, K., Liu, D., Niu, Y., and Lu, W. (2018). An optimization-based semantic building model generation method with a pilot case of a demolished construction. In: Chau K., Chan I., Lu W., and Webster C. (eds) *Proceedings of the 21st International Symposium on Advancement of Construction Management and Real Estate*. Springer, Singapore. doi:10.1007/978-981-10-6190-5_22.
- Yan, J., Jiang, W., and Shan, J. (2016). A global solution to topological reconstruction of building roof models from airborne LiDAR point clouds. *ISPRS Annals of Photogrammetry, Remote Sensing and Spatial Information Sciences*, 379-386. doi:10.5194/isprs-annals-III-3-379-2016.
- Yang, R. J., and Zou, P. X. (2016). Building integrated photovoltaics (BIPV): costs, benefits, risks, barriers and improvement strategy. *International Journal of Construction Management*, 16(1), 39-53. doi:10.1080/15623599.2015.1117709.
- You, R. J., and Lin, B. C. (2011). A quality prediction method for building model reconstruction using LiDAR data and topographic maps. *IEEE Transactions on Geoscience and Remote Sensing*, 49(9), 3471-3480. doi:10.1109/TGRS.2011.2128326.
- Zhang, W., Wang, H., Chen, Y., Yan, K., and Chen, M. (2014). 3D building roof modeling by optimizing primitive's parameters using constraints from LiDAR data and aerial imagery. *Remote Sensing*, 6(9), 8107-8133. doi:10.3390/rs6098107.
- Zhu, L., Lehtomäki, M., Hyypä, J., Puttonen, E., Krooks, A., and Hyypä, H. (2015). Automated 3D scene reconstruction from open geospatial data sources: Airborne laser scanning and a 2D topographic database. *Remote Sensing*, 7(6), 6710-6740. doi:10.3390/rs70606710.